

Original Research

Chronic Alcohol Exposure Alters the Levels and Assembly of the Actin Cytoskeleton and Microtubules in the Adult Mouse Hippocampus

Da-Peng Gao^{1,*}, Lu-Wan Wang², Dong-Lin Xie¹, Qiong Li³, Zhi-Peng Yu³, Zi-Hang Tang³, Ke-Ke Cui³, Yu Cai^{4,*}

Academic Editor: Gernot Riedel

Submitted: 5 December 2023 Revised: 31 January 2024 Accepted: 6 February 2024 Published: 19 June 2024

Abstract

Background: Alcohol abuse, a prevalent global health issue, is associated with the onset of cognitive impairment and neurodegeneration. Actin filaments (F-actin) and microtubules (MTs) polymerized from monomeric globular actin (G-actin) and tubulin form the structural basis of the neuronal cytoskeleton. Precise regulation of the assembly and disassembly of these cytoskeletal proteins, and their dynamic balance, play a pivotal role in regulating neuronal morphology and function. Nevertheless, the effect of prolonged alcohol exposure on cytoskeleton dynamics is not fully understood. This study investigates the chronic effects of alcohol on cognitive ability, neuronal morphology and cytoskeleton dynamics in the mouse hippocampus. Methods: Mice were provided *ad libitum* access to 5% (v/v) alcohol in drinking water and were intragastrically administered 30% (v/v, 6.0 g/kg/day) alcohol for six weeks during adulthood. Cognitive functions were then evaluated using the Y maze, novel object recognition and Morris water maze tests. Hippocampal histomorphology was assessed through hematoxylin-eosin (HE) and Nissl staining. The polymerized and depolymerized states of actin cytoskeleton and microtubules were separated using two commercial assay kits and quantified by Western blot analysis. Results: Mice chronically exposed to alcohol exhibited significant deficits in spatial and recognition memory as evidenced by behavioral tests. Histological analysis revealed notable hippocampal damage and neuronal loss. Decreased ratios of F-actin/G-actin and MT/tubulin, along with reduced levels of polymerized F-actin and MTs, were found in the hippocampus of alcohol-treated mice. Conclusions: Our findings suggest that chronic alcohol consumption disrupted the assembly of the actin cytoskeleton and MTs in the hippocampus, potentially contributing to the cognitive deficits and pathological injury induced by chronic alcohol intoxication.

Keywords: chronic alcoholic brain injury; cognitive deficit; actin cytoskeleton; microtubules; hippocampus

1. Introduction

Alcoholic beverages have been consumed throughout human history—celebrated for their role in social and cultural rituals. Despite pervasive usage, chronic excessive alcohol consumption carries a considerable burden, leading to alcohol abuse, dependence and severe impact on neural functions including learning, memory and cognition. Chronic alcoholic encephalopathy (CAE) often manifests in individuals with long-standing, heavy alcohol abuse, evidenced by central nervous system malnutrition, overt neurotoxicity and neurodegenerative changes [1–3]. Clinically, it is characterized by progressive cognitive impairments, ranging from attentional deficits and memory attrition to compromised executive function [4]. In severe cases, this culminates in alcoholic dementia or delirium [5,6]. Neuroanatomical studies have suggested that chronic alcohol ingestion correlates with shrinkage in the hippocampus, frontal cortices and midline thalamus, areas that are crucial for learning and memory processes, indicative of substantive neuronal loss [7,8].

At a cellular level, the orchestrated morphology and functionality of neurons are partially contingent upon intricate cytoskeletal protein dynamics. Within neuronal cells, actin exemplifies this dynamic, existing in a monomeric globular (G-actin) form, which polymerizes into a filamentous (F-actin) state. F-actin is notably concentrated within dendritic spines—micron-sized protrusions on dendrites that exhibit the majority of excitatory synapses in the mammalian brain. Any imbalance in the F-actin/G-actin ratio may be deleterious, distorting spine morphology and consequently synaptic function—events commonly associated with cognitive decline [9,10]. Parallels exist with tubulin, which oscillates between a free state and its polymeric form, microtubules (MTs). A well-maintained tubulin-MT equilibrium ensures effective signal transduction and intracellular trafficking within the axon [11]. Disruption of this balance, as seen with acetaldehyde (an ethanol metabolite) binding to tubulin, impairs microtubule assembly and interrupts crucial neuronal processes [12–14]. Alterations in MT-associated proteins, which promote microtubule as-

¹Department of Neurology, The First Affiliated Hospital of Ningbo University, 315020 Ningbo, Zhejiang, China

²School of Medical, Ningbo University, 315211 Ningbo, Zhejiang, China

³Department of Physiology and Pharmacology, School of Medicine, Ningbo University, 315211 Ningbo, Zhejiang, China

⁴Department of Pharmacy, Zhejiang Pharmaceutical University, 315500 Ningbo, Zhejiang, China

^{*}Correspondence: aresgdp@163.com (Da-Peng Gao); caiyuhk@163.com (Yu Cai)

sembly and stability, have been linked to the pathophysiology of neurocognitive disorders [15,16].

While previous studies have brought forward a substantial understanding of glutamate excitotoxicity and thiamine deficiency in the context of alcohol-induced neurotoxicity [3,17], less is known about how cytoskeletal disruption contributes to the cognitive impairments associated with alcohol use. The regulation of the dynamic assembly and spatial organization of the actin cytoskeleton and microtubules is crucial for maintaining neural functionality, yet whether chronic alcohol exposure directly impacts these structures within the hippocampus has seldom been probed in vivo. Prior in vitro analyses have shed light on how alcohol prompts cytoskeletal anomalies across various cell types, including neurons. For example, findings by Romero et al. [18,19] demonstrate that continuous alcohol exposure diminishes the quantity of both polymerized actin and tubulin in hippocampal neurons, alongside decreased activity of key guanosine triphosphatases (GT-Pases) of Ras homolog (Rho) family and altered dendritic spine morphology. Complementary research by Damuka et al. [20] corroborates that alcohol treatment (100 mM ethanol for three days) enhances MT stability while it concomitantly reduces tubulin monomers in SH-SY5Y neuroblastoma cells. Further, Tomás et al.'s [21-23] immunohistological studies have underscored that chronic alcohol intake disrupts an array of cellular functions including secretory and endocytic responses within astrocytes due to compromised actin and MT organization.

While these *in vitro* studies lay a valuable foundation, an empirical understanding of the repercussions of chronic alcohol exposure on the neuronal actin cytoskeleton and MTs assembly within a living organism has remained elusive. Here, this study bridges this gap by presenting *in vivo* evidence that characterizes the enduring effects of alcohol on the assembly of cytoskeletal components within the hippocampus, a region integral to cognitive processes. In the experimental design employed, a six-week regimen induced brain injury in mice to mimic chronic alcohol impairment. Detailed behavioral analyses were then performed to examine cognitive capacities, accompanied by histopathological and biochemical evaluations to gauge changes in neuronal morphology and to quantify the ratio of F-actin/G-actin and MT/tubulin.

2. Materials and Methods

2.1 Animals

Male C57BL/6J mice aged six to seven weeks were obtained from Zhejiang Vital River Laboratory Animal Technology Co., Ltd. (Pinghu, Zhejiang, China). The animals underwent a one-week adjustment phase in an environment with a consistent cycle of 12 hours of light and darkness at a stable temperature (25 \pm 1 °C). Experimental procedures were in strict adherence to the National Institutes of Health guidelines for laboratory animal care and

received approval from the Ningbo University Animal Care and Use Committee (IACUC-NBU20230138).

2.2 Experimental Design

An adult mouse model was constructed to simulate chronic alcohol-induced brain injury, refining a previously reported method by our team [24]. The protocol for establishing the mouse model during adulthood and conducting subsequent animal behavioral tests is illustrated in Fig. 1. The study population comprised forty mice randomly allocated into two groups of equal size: a control group and an alcohol-exposed group. Mice in the latter group were given 5% (v/v) ethanol freely via their drinking water, supplemented with a 30% (v/v) ethanol solution administered through gavage twice daily. The initial two weeks served as an acclimatization period with ethanol concentrations gradually increasing to 6.0 g/kg (1.2 g/kg for the first three days, 2.4 g/kg for days four to six, 3.6 g/kg for days seven to nine, 4.8 g/kg for days ten to twelve and 6.0 g/kg for days thirteen and fourteen), which was then sustained for the subsequent four weeks. Mice in the control group were administered water and received a normal diet and drinking water during all experiments. Subsequently, cognitive assessments were initiated via a suite of behavioral tests. Mice in the alcohol group continued to receive 5% (v/v) ethanol in their drinking water to mitigate withdrawal symptoms throughout the testing period, which included the Y maze, novel object recognition (NOR) and Morris water maze (MWM) tests. Sufficient rest was provided between tests, with intervals ranging from one to three days. After testing, all mice were euthanized, with eight from each group designated for brain histology and the remaining twelve earmarked for biochemical assays.

2.3 Behavior Tests

2.3.1 Y Maze

The Y maze test employed a previously described apparatus [25]. It consists of a three-armed maze set at 120-degree angles. Mice navigated the maze freely over a period of ten minutes, with entry patterns and total entries recorded during the final eight minutes. Consecutive entries into each distinct arm constituted an 'alternation', with alternation percentages reflecting spatial working memory and total arm entries providing insights into motor function.

2.3.2 Novel Object Recognition (NOR)

Following, with slight adjustments, the protocols of prior studies [26,27], the novel object recognition (NOR) test was transpired in a $25 \times 25 \times 25$ cm arena. Mice received a thirty-minute acclimation phase within this environment a day before the training phase. Two identical objects were presented for a ten-minute exploration session during the second day's training. One hour after training, a new object replaced one of the old, and mice were observed for their engagement with both the novel and famil-



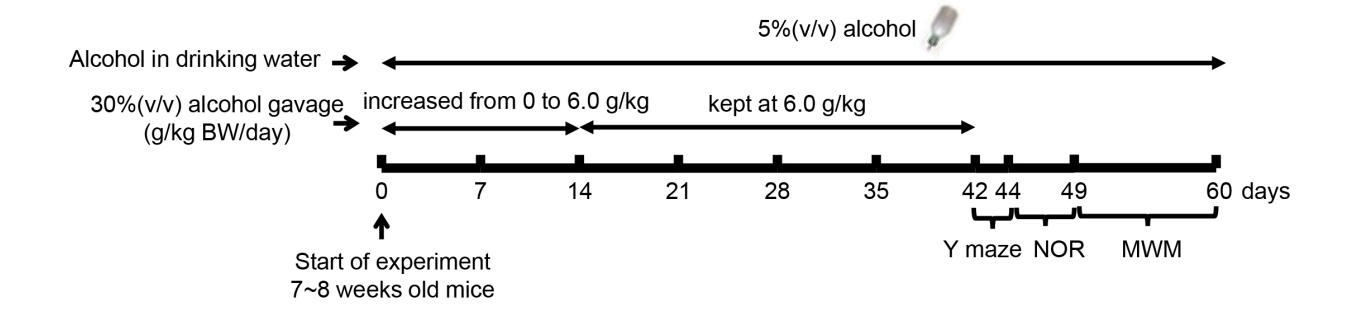


Fig. 1. Experimental protocol timeline for chronic alcohol exposure in adult C57BL/6J mice. Schedule of the experimental protocol illustrating the six week period of chronic alcohol administration used to induce brain injury in C57BL/6J mice, followed by the behavioral assessments. BW, body weight; NOR, novel object recognition; MWM, Morris water maze.

iar objects. The time spent interacting with these objects was documented. A mouse nose within a two centimeter distance or pointed at an object was considered 'investigation'. A NOR test discrimination index was derived as a measure of recognition memory and calculated as the ratio of the time difference between interacting with the new and known objects to the total time spent with both.

2.3.3 Morris Water Maze (MWM)

Carrying out the morris water maze (MWM) trials, adjusting for minor details, followed established practices [28,29]. Briefly, the assessment took place within a round basin measuring 100 cm across, containing an internal platform nine centimeters wide. The water temperature was kept at a consistent temperature ranging from 21 to 23 °C. The experiment was divided into three distinctive trials. The initial session was reserved for training using a visible platform, serving to familiarize mice with the environment and platform location. Mice that failed to locate the platform within sixty seconds were directed to it, given a twenty-second rest period, then allowed to orient themselves to the setup. The hidden platform training trial comprised two sessions a day and ran from the second to the sixth day. The platforms were placed in the same location, one centimeter beneath the water's surface when compared with the visual platform training trial. Mice were introduced to the round basin from various entry points to search for the submerged platform. The search duration time to platform discovery was recorded for each mouse. If a mouse failed to discover the platform within sixty seconds, it was guided to the location, given a twenty-second pause for rest, then allowed to familiarize itself with the environment. The space exploration trial began on the seventh day, where the platform had been removed. Mice were introduced into various quadrants of the pool, each time facing the of pool wall. The duration each mouse spent in the quadrant formerly containing the platform, the frequency of their crossings over the previous platform location and their movement patterns were all documented within a one-minute interval. The video tracking software, ANY-mazeTM (Stoelting, Wood Dale, IL, USA), was employed for recording and analyzing behavioral parameters.

2.4 Histological Examination

For histological analysis, mice underwent anesthesia with 1% pentobarbital sodium (P3761, Sigma-Aldrich, Shanghai, China) at a dosage of 80 mg per kilogram of body weight, followed by 0.9% saline via left ventricular perfusion. They were then fixed by perfusion with an icecold 4% paraformaldehyde solution. After being removed, mouse brains were fixed for an additional 18 hours at 4 °C in 4% paraformaldehyde. The sequential steps of paraffin embedding, sectioning, xylene dewaxing and ethanol gradient rehydration were followed, and the tissue slices were then stained with hematoxylin for a duration of five minutes. Subsequently, the slices were either re-stained with eosin for three minutes to complete the hematoxylin-eosin (HE) staining procedure or stained with 0.1% cresyl violet to complete the Nissl staining procedure. Stained brain slices were sequentially passed through ethanol and xylene and finally sealed with a neutral resin. Morphological changes in cortical and hippocampal neurons were observed using light microscopy (ECLIPSE Ci, Nikon, Tokyo, Japan) [30] and ImageJ software (v1.53, National Institutes of Health (NIH), Baltimore, MD, USA) was used to quantify neuronal numbers in images.

2.5 F-Actin/G-Actin in Vivo Assay

The G-actin/F-actin *in vivo* assay kit (BK037, Cytoskeleton, Denver, CO, USA) was employed to differentiate F- and G-actin, in alignment with the instructions provided by the kit's manufacturer. Briefly, fresh hippocampal tissue was homogenized on ice with ten times the volume of lysis buffer and F-actin stabilization buffer containing 1 mM ATP and a protease inhibitor cocktail (PIC02, Cytoskeleton). The resultant tissue lysate was then double centrifuged ($400 \times g$, 10 min, 4 °C) and the liquid supernatant was carefully pipetted into well-labeled ultracen-



trifugation tubes. The clear supernatant underwent an additional round of centrifugation (100,000 ×g, 60 min, 4 °C). Subsequently, the supernatant containing G-actin was promptly separated from the pellet containing F-actin and was immediately chilled on ice. The gathered pellet, which was concentrated with F-actin, was reconstituted in an Factin depolymerizing buffer, followed by a sixty-minute incubation on ice. The suspension was mixed every fifteen minutes during the incubation period to completely depolymerize the F-actin. Total protein contents present in each sample were determined using a bicinchoninic acid (BCA) protein assay kit (PC0020, Solarbio, Beijing, China). Ten micrograms of protein from the G-actin and F-actin fractions of each sample were lysed in Sodium dodecyl sulfate (SDS) sample buffer (SDS01, Cytoskeleton) and incubated at 85 °C for five minutes before being separated on a 12% SDS polyacrylamide gel and subsequently transferred onto polyvinylidene difluoride (PVDF) membranes. The membranes were treated with 5% non-fat milk in Tris buffered saline with Tween (TBST) for thirty minutes to prevent non-specific binding and then incubated with an anti-actin primary antibody (AAN02, dilution 1:1000, Cytoskeleton) at 4 °C overnight. Following this, the membranes underwent three washes, each lasting ten minutes. They were then exposed to an anti-mouse secondary antibody (SA00001-1, dilution 1:5000, Proteintech, Rosemont, IL, USA) for one hour at ambient temperature. The target protein band was visualized by enhanced chemiluminescence (ECL) Western Blotting Detection Reagents (P10100, nembio, Suzhou, Jiangsu, China) and detected using a chemiluminescence scanner (Chemi Dog Imaging System, Tanon 5300M, Shanghai, China). Densitometric analysis was performed to quantify the band intensity using ImageJ software (v1.53, National Institutes of Health (NIH), Baltimore, MD, USA).

2.6 MT/Tubulin in Vivo Assay

MT and unbound tubulin were segregated using a dedicated MT/tubulin in vivo assay kit (BK038, Cytoskeleton), following the manufacturer guidelines. To ensure the stability of microtubules, all apparatus rotors, centrifuge tubes and buffers were warmed to 37 °C prior to use. Briefly, approximately 20 mg of each hippocampal tissue sample was homogenized at 37 °C with 300 µL lysis microtubule stabilization buffer containing 1 mM ATP, 0.1 mM GTP and protease inhibitor cocktail (PIC02, Cytoskeleton). This tissue lysate was briefly vortexed before undergoing centrifugal separation (1000 ×g, 5 min, 37 °C). Following this, the supernatant obtained at low speed was gently transferred to a fresh tube and maintained at 37 °C. The low-speed pellet (P1 fraction) containing microtubules was resuspended in 200 µL radio-immunoprecipitation assay (RIPA) buffer (R0020, Solarbio, Beijing, China) which contained 1% SDS. The low-speed supernatant from each sample was centrifuged at 100,000 ×g for 30 minutes at

37 °C. The resulting high-speed supernatant (S2 fraction) containing soluble tubulin was transferred to another tube. The high-speed pellet (P2 fraction) containing microtubules was then resuspended in 200 µL microtubule depolymerization buffer. The P1, P2 and S2 fractions of each sample then underwent BCA protein quantification. From each sample fraction, ten micrograms of protein were lysed using SDS sample buffer (SDS01, Cytoskeleton), followed by incubation at 85 °C for five minutes. Afterward, proteins were resolved on a 12% SDS polyacrylamide gel and then transferred to PVDF membranes. The membranes were saturated with 5% non-fat milk in TBST for a duration of thirty minutes and then subjected to an overnight incubation (4 °C) with the anti-tubulin antibody (ATN02, 1:1000, Cytoskeleton). Membranes then underwent a one-hour incubation at ambient temperature with anti-sheep secondary antibody (GL21, dilution 1:10,000, Cytoskeleton). The target protein band was visualized by ECL Western Blotting Detection Reagents (P10100, ncmbio) and imaged using a Chemi Dog Imaging System (Tanon 5300M, Shanghai, China). Densitometric analysis using ImageJ (v1.53, NIH) allowed for the quantification of band intensity. The total MT content was determined by summing the MT amounts present in the P1 and P2 fractions.

2.7 Statistical Analysis

Results are reported as the mean \pm standard error of the mean (SEM). GraphPad Prism (version 9.0, GraphPad Software, San Diego, CA, USA) was employed for statistical analysis and graphical plotting. Four tests were utilized to evaluate the conformity of the variable distribution to a normal (Gaussian) distribution, including the D'Agostino & Pearson test, the Anderson-Darling test, the Shapiro-Wilk test, and the Kolmogorov-Smirnov test. Differences in means were determined by unpaired t-tests and effect sizes were calculated using Cohen's d. Escalations in body weight and escape latency during the hidden platform MWM trial were subjected to repeated measures analysis of variance (ANOVA) with Bonferroni post-tests. Detailed reporting included F, t, p-values, degrees of freedom and additional effect size metrics. Statistical significance was established at p < 0.05.

3. Results

3.1 Chronic Alcohol-Induced Cognitive Impairment in Mice

Over a period of six weeks of alcohol exposure, mice in the alcohol group exhibited a trend toward lower body weight when compared to controls; however, the disparity did not reach statistical significance (Fig. 2A, factor of groups: $F_{(1,38)} = 4.152$, p = 0.0550 or groups × days interaction: $F_{(6,228)} = 2.089$, p = 0.0594) according to repeated measures ANOVA.

Behavioral assessments were employed to evaluate cognitive deficits in alcohol-exposed mice. The Y maze



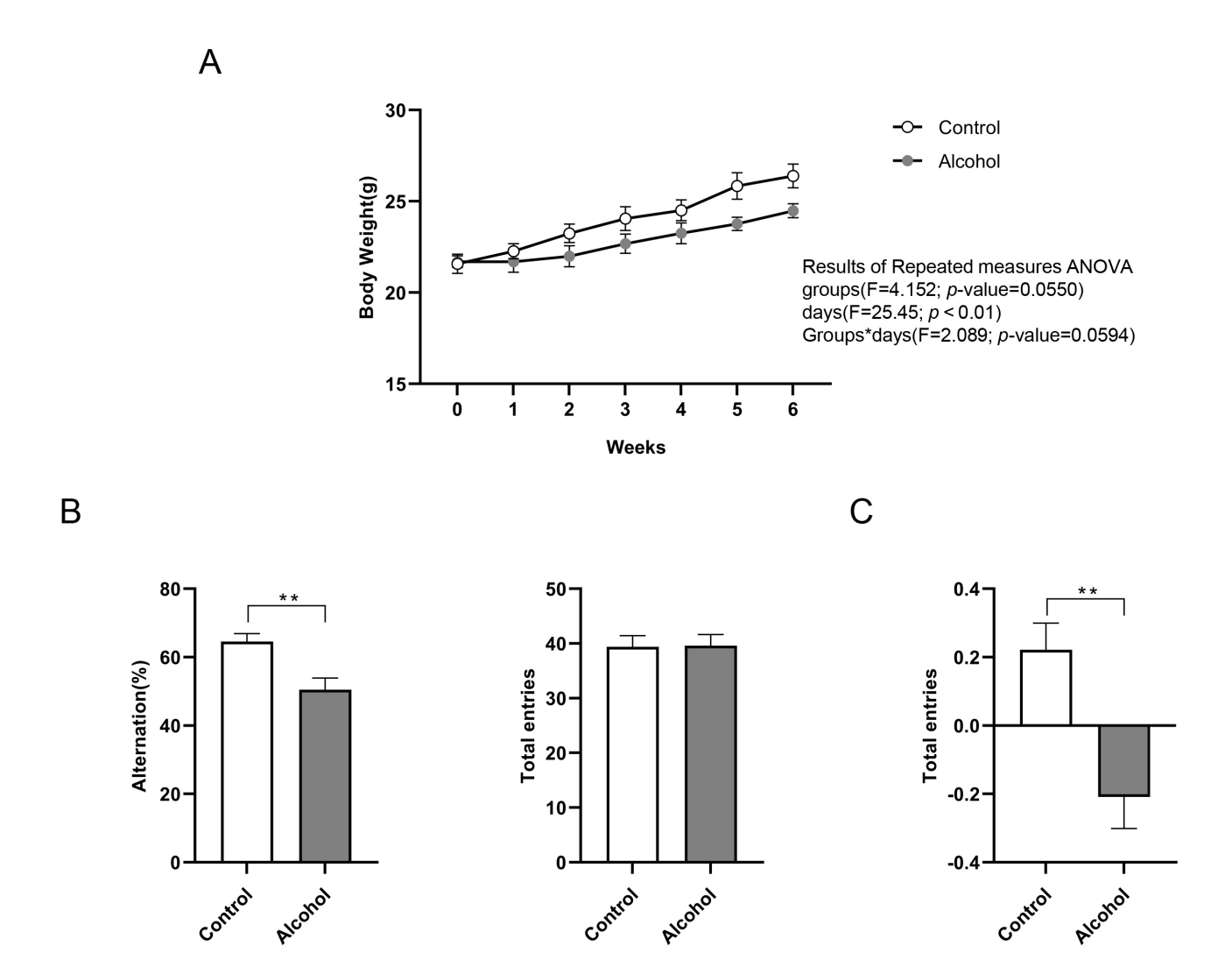


Fig. 2. Impact of chronic alcohol consumption on behavioral test outcomes in mice. (A) Trajectory of body weight modifications across a six-week span. (B) Percentage of correct alternations and the total number of arm entries in the Y maze test. (C) Discrimination index in the NOR test. All data are presented as mean \pm SEM for n=20 mice per experimental group. Statistical significance of the differences between the chronic alcohol group and the control group was analyzed using unpaired t-tests, denoted by **p < 0.01. ANOVA, analysis of variance; SEM, standard error of the mean.

test, a measure of spatial working memory and exploration, revealed a statistically significant decrease in spontaneous alternation percentage in the alcohol group ($t_{(38)} = 2.973$, p < 0.01, d = 0.9401, Fig. 2B), indicative of impaired short-term spatial working memory due to chronic alcohol treatment. There was no significant difference in the number of arm entries, which suggests that exploratory behavior remained unaffected (Fig. 2B).

The NOR test was used to investigate recognition memory. Alcohol-treated mice demonstrated a notable impairment in their ability to recognize novel objects compared to controls ($t_{(38)} = 3.536$, p < 0.01, d = 1.118, Fig. 2C). The results of the NOR test indicated a profound deficit in object recognition memory attributed to chronic alcohol exposure.

Spatial learning and memory were probed utilizing the classic MWM test. In the initial visible platform trial, aimed at eliminating the potential influence of sensorimotor or motivational impairments, no significant differences between groups were detected in either escape latency or swimming velocity (Fig. 3A). Across the subsequent hidden platform trials, spanning days two to six, although both groups demonstrated a reduction in escape latency over time, the alcohol group persistently exhibited longer latencies, with a significant discrepancy emerging between the two groups, as evidenced by a repeated measures ANOVA (Fig. 3B, factor of group: $F_{(1,38)} = 3.526$, p < 0.05). Compared with the control group, there was a significant prolongation in escape latency for the alcohol group on days five and six when analyzed with Bonferroni post hoc comparison (5th day, $t_{(38)} = 2.752$, p < 0.05, d = 0.8703; 6th



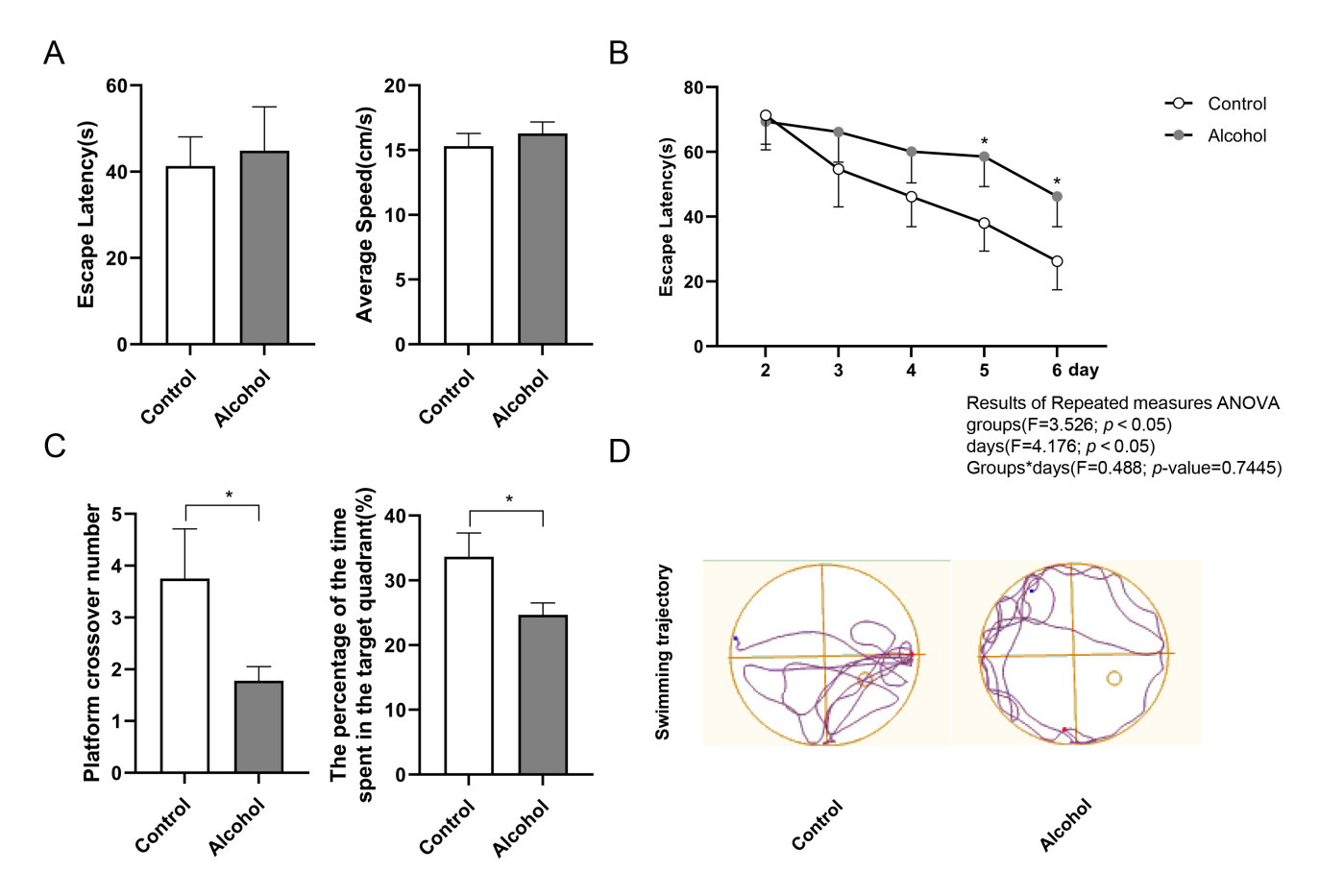


Fig. 3. Effect of chronic alcohol consumption on Morris water maze test performance in mice. (A) Escape latency and swimming velocity during the visible platform trials conducted on day one. (B) Escape latencies over a series of hidden platform trials from days two to six with data analyzed using two-way ANOVA with repeated measures; *p < 0.05 indicates significance compared to the control group after Bonferroni *post hoc* testing. (C) Number of platform crosses and the percentage of time spent in the target quadrant on the probe trial day seven using an unpaired t-test for statistical comparison; *p < 0.05 compared with the control group. (D) Swimming trajectorymap during the probe trial with blue markers indicating entry points and red markers delineating exit points from the water. Mean \pm SEM values are reported for n = 20 mice per group.

day, $t_{(38)} = 2.726$, p < 0.05, d = 0.8620, Fig. 3B). During the probe trial on day seven, the number of platform crossings ($t_{(38)} = 2.632$, p < 0.01, d = 0.8323, Fig. 3C) and the proportion of time spent in the target quadrant ($t_{(38)} = 2.027$, p < 0.01, d = 0.6410, Fig. 3C) were significantly lower in the alcohol-exposed group. For the search strategy, the trajectories of the alcohol mice were less concentrated in the target quadrant (Fig. 3D). Collectively, these observations suggest that ethanol exposure is deleterious to both spatial and recognition memory.

3.2 Chronic Alcohol Caused Pathological Damage in the Hippocampus of Mice

HE staining disclosed stark differences in neuronal arrangement and structure between the control and alcoholexposed groups. Neuronal shrinkage and deformation were apparent in the latter (Fig. 4A). Nissl staining corroborated these pathological disparities (Fig. 4B). Quantitative analyses revealed significant reductions in neuronal counts

within the CA1 region of the hippocampus of alcoholtreated mice in both HE ($t_{(14)} = 2.156$, p < 0.05, d = 0.8802, Fig. 4C) and Nissl-stained sections ($t_{(14)} = 5.421$, p < 0.001, d = 2.213, Fig. 4D), indicative of alcohol-induced neurodegeneration.

3.3 Chronic Alcohol Alters Actin and Tubulin Polymerization

Two biochemical assays were utilized to examine the impact of chronic alcohol on cytoskeletal integrity, specifically the polymerization capacities of actin and tubulin within the hippocampus. A significant decline in the F-actin/G-actin ratio was observed ($t_{(22)} = 3.767$, p < 0.01, d = 1.884, Fig. 5C), resulting from a reduction in F-actin ($t_{(22)} = 2.903$, p < 0.01, d = 1.452, Fig. 5A) and an increase in G-actin levels ($t_{(22)} = 3.014$, p < 0.01, d = 1.507, Fig. 5A). Chronic alcohol exposure was also associated with a diminished MT/tubulin ratio ($t_{(22)} = 2.097$, p < 0.05, d = 1.049, Fig. 5C), reflecting a reduction in polymerized MT ($t_{(22)} = 5.000$).



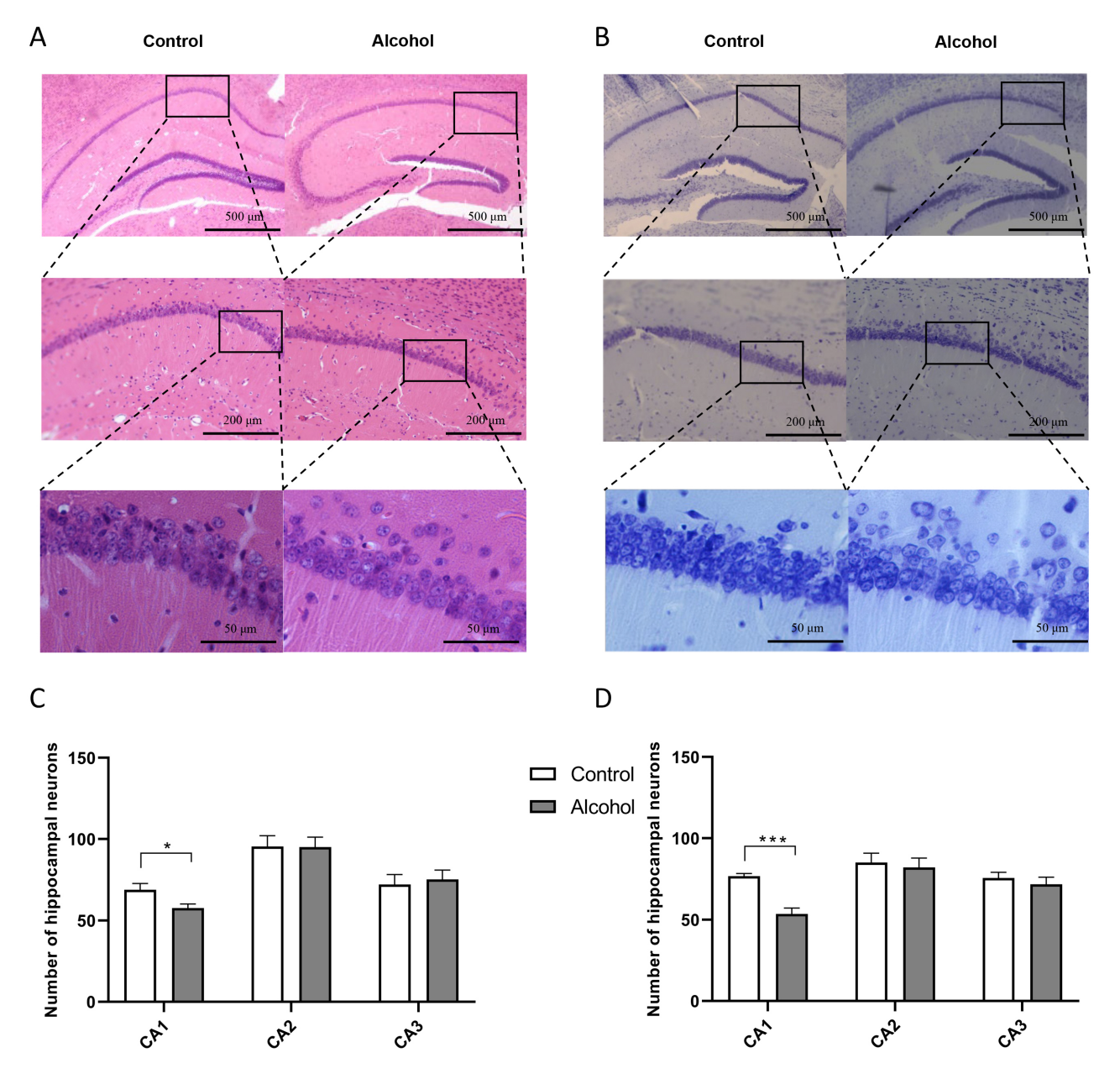


Fig. 4. Effect of chronic alcohol exposure on neuronal pathology in mouse hippocampus. (A) HE stained hippocampal neurons. (B) Nissl stained hippocampal neurons. (C,D) Quantitative analyses of neuronal counts in CA1, CA2 and CA3 regions of the hippocampus in the images stained with HE and Nissl, respectively. Data are shown as mean \pm SEM for n = 8 subjects per group. Statistically significant differences from the control group are indicated by *p < 0.05, ***p < 0.001 (unpaired t-test). HE, hematoxylin-eosin.

= 2.081, p < 0.05, d = 1.041, Fig. 5B), without a significant alteration in free tubulin levels. These findings suggest that chronic alcohol exposure leads to the destabilization of both actin filaments and microtubules in the hippocampus, which could underpin the observed cognitive deficits.

4. Discussion

Chronic alcohol-induced brain injury is an enduring affliction that impairs multiple regions within the brain, notably the hippocampus, leading to a spectrum of cognitive deficits, memory loss, altered mental state and dys-

praxia [31–34]. Common rodent models for alcohol-related toxic brain injury include exposure by drinking [35], intraperitoneal [36] or intragastric injections [37,38], and vapor chambers [39]. In general, acute and binge-like experimental protocols for alcohol administration often utilize intraperitoneal and intragastric methods, whereas approaches such as free-choice drinking and vapor inhalation are typically reserved for studies requiring prolonged periods of alcohol exposure [40].

In this study, a hybrid approach was utilized to induce alcohol intoxication and brain injury in adult mice



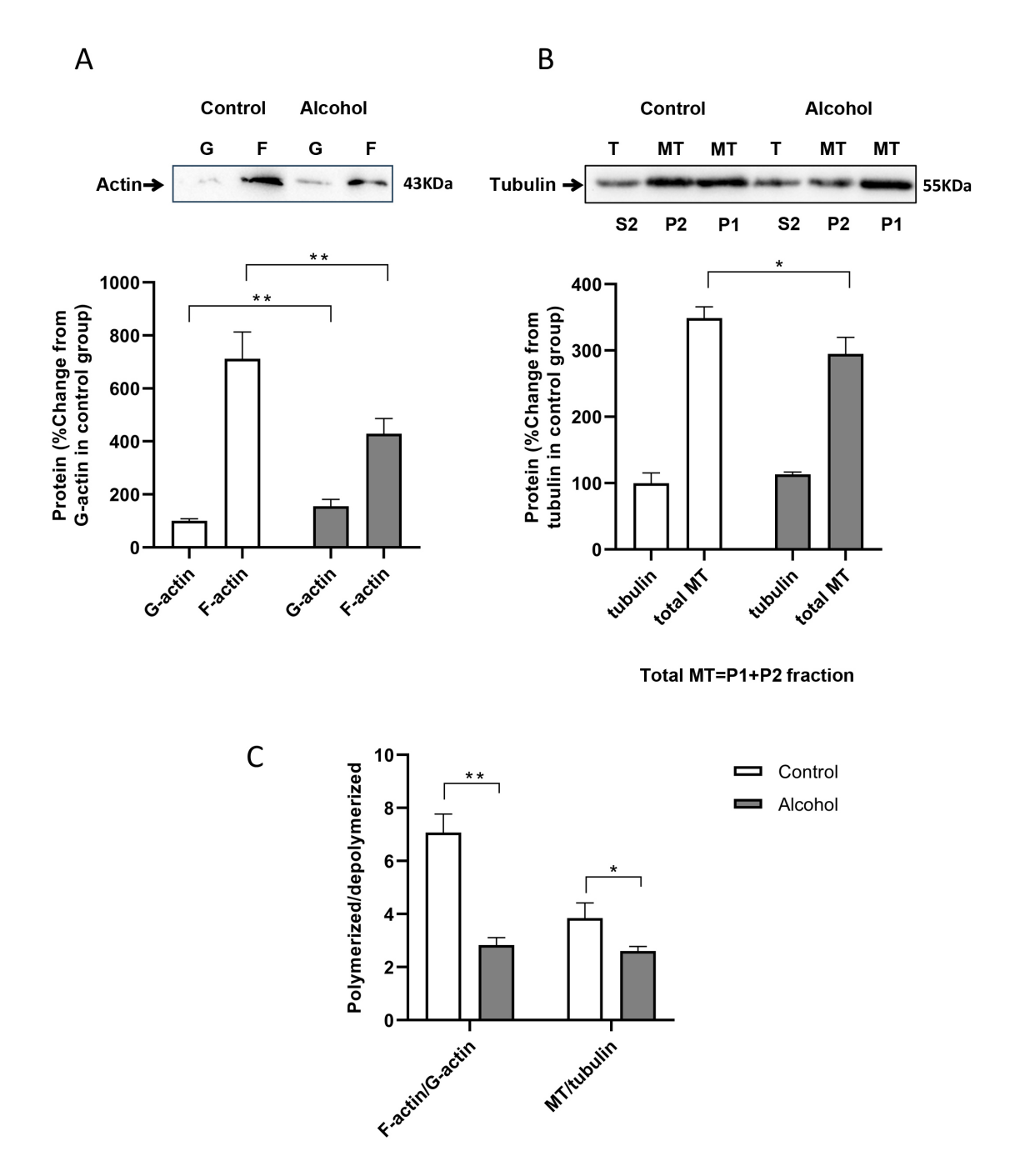


Fig. 5. Alterations in filamentous actin and microtubule levels and assembly in the hippocampus post-chronic alcohol consumption. (A) The relative abundance of G-actin and F-actin, with G representing globular actin and F denoting filamentous actin. (B) The levels of tubulin and microtubules; following subcellular fractionation, hippocampal tissues were separated into fractions P1 and P2 (comprising MT) and fraction S2 (containing free tubulin), with total MT defined as P1+P2. (C) The impact of alcohol on actin cytoskeleton and microtubule assembly, calculating F-actin/G-actin and MT/tubulin ratios using densitometric analysis. Data are represented as mean \pm SEM for groups of 12 mice. *p < 0.05, **p < 0.01 compared with the control group. MT, microtubule.

This method, which was previously published with minor modifications [24], combines intragastric gavage and voluntary consumption. The following are the characteristics of this mice model. Firstly, according to the definition provided by the National Institute on Alcohol Abuse and Alcoholism (NIAAA), risky use of alcohol is characterized by men under 65 years old consuming more than four standard

drinks of ethanol per day or alcohol intake exceeding 0.8 g/kg/day. A conversion factor of 12.3 was calculated between the experimental mice and humans, indicating that a mouse should consume over 10.5 g/kg/day, based on a 25 g mouse body weight. Initially, alcohol was administered solely through gavage, but encountered a high mortality rate among the model animals. However, allowing the



mice to consume alcohol solely by drinking did not guarantee reaching a toxic blood alcohol concentration. Moreover, binge-like ethanol administration causes greater brain damage compared to continuous exposure. This justifies the strategy employed by this study where voluntary and involuntary alcohol consumption were combined. The mice were administered 6 g/kg of alcohol through gavage and 4.5–9 g/kg through drinking. The dosage and concentration of alcohol in the gavage solution and drinking water were determined based on the results of our preliminary study.

Acknowledging the limitations of this model is critical for interpreting the findings. Notably, the monitoring of blood alcohol levels resulting from daily consumption were omitted, which, according to the estimates in the literature, could have peaked at 400 mg/dL [41,42]. Additionally, the potential systemic damage to organs such as the liver or gastrointestinal tract was not assessed, leaving a partial view of the overall alcohol impact. Finally, the difference in daily calorie intake between the control group and the alcohol group. Based on simplified calculations, mice in the alcohol group ingest approximately 7.0-10.5% of their total calories as ethanol. The caloric intake between the two groups is similar, but not identical. With this model in place, this study demonstrated that chronic alcohol exposure precipitated cognitive dysfunction and concomitant hippocampal pathology, concurring with lowered F-actin/G-actin and MT/tubulin ratios. The evidence prompts a compelling hypothesis that these deficits stem, at least in part, from maladaptations in cytoskeletal proteins assembly. Offenhäuser et al. [43] discovered that mice deficient in Eps8, a crucial regulator of actin dynamics, showed heightened resistance to and consumption of ethanol. They examined the mechanism in cultured cerebellar granule neurons and proposed that modifications in actin dynamics could impact alcohol resistance. Tomás M et al. [21] demonstrated that lysophosphatidic acid therapy prevented alcohol-induced defects in the actin cytoskeleton and microtubule organization in rat astrocytes. Numerous Rho guanosine triphosphatases (Rho GTPases) regulate neuronal cytoskeleton dynamics. Rho-associated protein kinases (ROCKs) are currently the most detailed and important downstream target effector molecules of Rho GTPases [44,45]. Downregulation of ROCK2 relieved chronic alcohol-induced cognitive deficits by exerting anti-apoptotic, anti-inflammatory, and antioxidative effects [46]. Such evidence suggests that impaired cytoskeleton dynamics potentially contribute to chronic alcohol-induced cognitive deficits. Thus, restoring cytoskeleton dynamics could be a promising treatment strategy to counteract the cognitive deficits induced by chronic alcohol consumption.

5. Conclusions

In this study, it was observed that prolonged alcohol exposure led to cognitive impairment and morphological irregularities in the hippocampus of adult mice. Additionally,

chronic alcohol exposure resulted in changes in the levels and assembly of F-actin and microtubules in the hippocampus. As a result, it is hypothesized that chronic alcohol exposure disrupts the assembly of the actin cytoskeleton and microtubules in the hippocampus, potentially contributing to the cognitive deficits and pathological damage induced by chronic alcohol consumption.

Abbreviations

CAE, chronic alcoholic encephalopathy; F-actin, actin filaments; MT, microtubule; NOR, novel object recognition; MWM, morris water maze; GTPases, guanosine triphosphatases; ROCK, Rho-associated protein kinases.

Availability of Data and Materials

The datasets used and/or analyzed during the current study are available from the corresponding author on reasonable request.

Author Contributions

DG and YC designed the research study. DG, YC, LW and DX conducted the experiment. DG, YC, QL, KC, ZY and ZT analyzed and interpreted the data. DG and YC wrote the manuscript draft and made the revision. All authors contributed to editorial changes in the manuscript. All authors read and approved the final manuscript. All authors have participated sufficiently in the work and agreed to be accountable for all aspects of the work.

Ethics Approval and Consent to Participate

The animal experiments were conducted in accordance with the National Institutes of Health Guide for the Care and Use of Laboratory Animals and were approved by the Animal Care and Use Committee of Ningbo University (IACUC-NBU20230138).

Acknowledgment

We would like to thank Professor hao-wei Shen's lab, Department of Physiology and Pharmacology, School of Medicine, Ningbo University, for providing technical research facilities. We would also like to thank Professor haowei Shen, who read and made very useful comments on our manuscript.

Funding

This research was supported by Ningbo Natural Science Foundation (Project ID: 202003N4245 and 2023J139) for Da-Peng Gao, and Zhejiang Provincial Natural Science Foundation of China under Grant No. LGF21H090016, Ningbo Natural Science Foundation (Project ID: 2023J305) for Yu Cai.

Conflict of Interest

The authors declare no conflict of interest.



References

- de la Monte SM, Kril JJ. Human alcohol-related neuropathology. Acta Neuropathologica. 2014; 127: 71–90.
- [2] Topiwala A, Ebmeier KP. Effects of drinking on late-life brain and cognition. Evidence-based Mental Health. 2018; 21: 12–15.
- [3] Langlais PJ, Zhang SX, Savage LM. Neuropathology of thiamine deficiency: an update on the comparative analysis of human disorders and experimental models. Metabolic Brain Disease. 1996; 11: 19–37.
- [4] Vetreno RP, Hall JM, Savage LM. Alcohol-related amnesia and dementia: animal models have revealed the contributions of different etiological factors on neuropathology, neurochemical dysfunction and cognitive impairment. Neurobiology of Learning and Memory. 2011; 96: 596–608.
- [5] Caneva S, Ottonello M, Torselli E, Pistarini C, Spigno P, Fiabane E. Cognitive Impairments in Early-Detoxified Alcohol-Dependent Inpatients and Their Associations with Socio-Demographic, Clinical and Psychological Factors: An Exploratory Study. Neuropsychiatric Disease and Treatment. 2020; 16: 1705–1716.
- [6] Khalifa N, Magee T, Shirazi S, Salman S, Yang CC, Mela M. The neurocognitive profiles of justice involved people with foetal alcohol spectrum disorder: A systematic review. Behavioral Sciences & the Law. 2022; 40: 87–111.
- [7] Karoly HC, Skrzynski CJ, Moe EN, Bryan AD, Hutchison KE. Exploring relationships between alcohol consumption, inflammation, and brain structure in a heavy drinking sample. Alcoholism, Clinical and Experimental Research. 2021; 45: 2256– 2270.
- [8] Savage LM, Nunes PT, Gursky ZH, Milbocker KA, Klintsova AY. Midline Thalamic Damage Associated with Alcohol-Use Disorders: Disruption of Distinct Thalamocortical Pathways and Function. Neuropsychology Review. 2021; 31: 447–471.
- [9] Chazeau A, Giannone G. Organization and dynamics of the actin cytoskeleton during dendritic spine morphological remodeling. Cellular and Molecular Life Sciences. 2016; 73: 3053–3073.
- [10] Sikora E, Bielak-Zmijewska A, Dudkowska M, Krzystyniak A, Mosieniak G, Wesierska M, et al. Cellular Senescence in Brain Aging. Frontiers in Aging Neuroscience. 2021; 13: 646924.
- [11] Hohmann T, Dehghani F. The Cytoskeleton-A Complex Interacting Meshwork. Cells. 2019; 8: 362.
- [12] Sorrell MF, Tuma DJ. Hypothesis: alcoholic liver injury and the covalent binding of acetaldehyde. Alcoholism, Clinical and Experimental Research. 1985; 9: 306–309.
- [13] Smith SL, Jennett RB, Sorrell MF, Tuma DJ. Acetaldehyde substoichiometrically inhibits bovine neurotubulin polymerization. The Journal of Clinical Investigation. 1989; 84: 337–341.
- [14] Pratt OE, Rooprai HK, Shaw GK, Thomson AD. The genesis of alcoholic brain tissue injury. Alcohol and Alcoholism. 1990; 25: 217–230.
- [15] Gozes I. Microtubules (tau) as an emerging therapeutic target: NAP (davunetide). Current Pharmaceutical Design. 2011; 17: 3413–3417.
- [16] Avdoshina V, Mahoney M, Gilmore SF, Wenzel ED, Anderson A, Letendre SL, et al. HIV influences microtubule associated protein-2: potential marker of HIV-associated neurocognitive disorders. AIDS. 2020; 34: 979–988.
- [17] Rao R, Topiwala A. Alcohol use disorders and the brain. Addiction. 2020; 115: 1580–1589.
- [18] Romero AM, Esteban-Pretel G, Marín MP, Ponsoda X, Ballestín R, Canales JJ, *et al.* Chronic ethanol exposure alters the levels, assembly, and cellular organization of the actin cytoskeleton and microtubules in hippocampal neurons in primary culture. Toxicological Sciences. 2010; 118: 602–612.
- [19] Romero AM, Renau-Piqueras J, Pilar Marin M, Timoneda J, Berciano MT, Lafarga M, et al. Chronic alcohol alters dendritic

- spine development in neurons in primary culture. Neurotoxicity Research. 2013; 24: 532–548.
- [20] Damuka N, Orr M, Czoty PW, Weiner JL, Martin TJ, Nader MA, et al. Effect of ethanol and cocaine on [11C]MPC-6827 uptake in SH-SY5Y cells. Molecular Biology Reports. 2021; 48: 3871– 3876
- [21] Tomás M, Lázaro-Diéguez F, Durán JM, Marín P, Renau-Piqueras J, Egea G. Protective effects of lysophosphatidic acid (LPA) on chronic ethanol-induced injuries to the cytoskeleton and on glucose uptake in rat astrocytes. Journal of Neurochemistry. 2003; 87: 220–229.
- [22] Tomás M, Durán JM, Lázaro-Diéguez F, Babià T, Renau-Piqueras J, Egea G. Fluorescent analogues of plasma membrane sphingolipids are sorted to different intracellular compartments in astrocytes; Harmful effects of chronic ethanol exposure on sphingolipid trafficking and metabolism. FEBS Letters. 2004; 563: 59–65.
- [23] Tomás M, Marín P, Megías L, Egea G, Renau-Piqueras J. Ethanol perturbs the secretory pathway in astrocytes. Neurobiology of Disease. 2005; 20: 773–784.
- [24] Cai Y, Wang LW, Xie DL, Gao DP. Establishment of chronic alcoholic brain injury model in mice. Chinese Journal of Comparative Medicine. 2023; 33: 71–77. (In Chinese)
- [25] Detrait E, Maurice T, Hanon E, Leclercq K, Lamberty Y. Lack of synaptic vesicle protein SV2B protects against amyloid-β₂₅₋₃₅induced oxidative stress, cholinergic deficit and cognitive impairment in mice. Behavioural Brain Research. 2014; 271: 277– 285.
- [26] Lueptow LM. Novel Object Recognition Test for the Investigation of Learning and Memory in Mice. Journal of Visualized Experiments: JoVE. 2017; 55718.
- [27] Choi SY, Han K, Cutforth T, Chung W, Park H, Lee D, et al. Mice lacking the synaptic adhesion molecule Neph2/Kirrel3 display moderate hyperactivity and defective novel object preference. Frontiers in Cellular Neuroscience. 2015; 9: 283.
- [28] Ding N, Jiang J, Xu A, Tang Y, Li Z. Manual Acupuncture Regulates Behavior and Cerebral Blood Flow in the SAMP8 Mouse Model of Alzheimer's Disease. Frontiers in Neuroscience. 2019; 13: 37.
- [29] Tian H, Ding N, Guo M, Wang S, Wang Z, Liu H, *et al.* Analysis of Learning and Memory Ability in an Alzheimer's Disease Mouse Model using the Morris Water Maze. Journal of Visualized Experiments. 2019; e60055.
- [30] Wang B, Huang X, Pan X, Zhang T, Hou C, Su WJ, *et al.* Minocycline prevents the depressive-like behavior through inhibiting the release of HMGB1 from microglia and neurons. Brain, Behavior, and Immunity. 2020; 88: 132–143.
- [31] Harper C. The neuropathology of alcohol-related brain damage. Alcohol and Alcoholism. 2009; 44: 136–140.
- [32] Sachdeva A, Chandra M, Choudhary M, Dayal P, Anand KS. Alcohol-Related Dementia and Neurocognitive Impairment: A Review Study. International Journal of High Risk Behaviors & Addiction. 2016; 5: e27976.
- [33] Bates ME, Bowden SC, Barry D. Neurocognitive impairment associated with alcohol use disorders: implications for treatment. Experimental and Clinical Psychopharmacology. 2002; 10: 193–212.
- [34] Green A, Garrick T, Sheedy D, Blake H, Shores EA, Harper C. The effect of moderate to heavy alcohol consumption on neuropsychological performance as measured by the repeatable battery for the assessment of neuropsychological status. Alcoholism, Clinical and Experimental Research. 2010; 34: 443–450
- [35] Xu S, Zhu W, Wan Y, Wang J, Chen X, Pi L, *et al.* Decreased Taurine and Creatine in the Thalamus May Relate to Behavioral Impairments in Ethanol-Fed Mice: A Pilot Study of Proton Mag-



- netic Resonance Spectroscopy. Molecular Imaging. 2018; 17: 1536012117749051.
- [36] Liew HK, Cheng HY, Huang LC, Li KW, Peng HF, Yang HI, *et al.* Acute Alcohol Intoxication Aggravates Brain Injury Caused by Intracerebral Hemorrhage in Rats. Journal of Stroke and Cerebrovascular Diseases. 2016; 25: 15–25.
- [37] Luo J, Shen Z, Chen G, Wang D, Yu X. Pontine Changes in Metabolites and Axonal Fibres of Rats Following Four-week Alcohol Exposure: In Vivo Diffusion Tensor Imaging and 1h-magnetic Resonance Spectroscopy Study at 7.0 T. Alcohol and Alcoholism. 2017; 52: 145–150.
- [38] Zahr NM, Carr RA, Rohlfing T, Mayer D, Sullivan EV, Colrain IM, *et al*. Brain metabolite levels in recently sober individuals with alcohol use disorder: Relation to drinking variables and relapse. Psychiatry Research. Neuroimaging. 2016; 250: 42–49.
- [39] Frischknecht U, Hermann D, Tunc-Skarka N, Wang GY, Sack M, van Eijk J, et al. Negative Association Between MR-Spectroscopic Glutamate Markers and Gray Matter Volume After Alcohol Withdrawal in the Hippocampus: A Translational Study in Humans and Rats. Alcoholism, Clinical and Experimental Research. 2017; 41: 323–333.
- [40] Bell RL, Hauser SR, Liang T, Sari Y, Maldonado-Devincci A, Rodd ZA. Rat animal models for screening medications to treat alcohol use disorders. Neuropharmacology. 2017; 122: 201–

- 243.
- [41] Livy DJ, Parnell SE, West JR. Blood ethanol concentration profiles: a comparison between rats and mice. Alcohol. 2003; 29: 165–171.
- [42] Cook RT, Schlueter AJ, Coleman RA, Tygrett L, Ballas ZK, Jerrells TR, et al. Thymocytes, pre-B cells, and organ changes in a mouse model of chronic ethanol ingestion—absence of subset-specific glucocorticoid-induced immune cell loss. Alcoholism, Clinical and Experimental Research. 2007; 31: 1746–1758.
- [43] Offenhäuser N, Castelletti D, Mapelli L, Soppo BE, Regondi MC, Rossi P, et al. Increased ethanol resistance and consumption in Eps8 knockout mice correlates with altered actin dynamics. Cell. 2006; 127: 213–226.
- [44] Hodge RG, Ridley AJ. Regulating Rho GTPases and their regulators. Nature Reviews. Molecular Cell Biology. 2016; 17: 496–510
- [45] Gray JL, von Delft F, Brennan PE. Targeting the Small GTPase Superfamily through Their Regulatory Proteins. Angewandte Chemie. 2020; 59: 6342–6366.
- [46] Li X, Tong J, Liu J, Wang Y. Down-regulation of ROCK2 alleviates ethanol-induced cerebral nerve injury partly by the suppression of the NF-κB signaling pathway. Bioengineered. 2020; 11: 779–790.

